Enhanced permeability and fouling-resistant capacity of poly(vinylidene fluoride) ultrafiltration membrane based on the PPG-co-PEG-co-PPG copolymer with two hydrophobic terminals and one hydrophilic intermediate

Bo Zhang, Panpan Wang, Jianxin Yu, Haicheng Jiang, Po Gao and Jun Ma

ABSTRACT

A simple and efficient route was used to prepare an amphiphilic copolymer (poly(propylene glycol)-co-poly(ethylene glycol)-co-poly(propylene glycol)) (PPG-co-PEG-co-PPG) by one-pot polymerization reaction. This copolymer was used as the hydrophilic additive in preparation of poly(vinylidene fluoride) (PVDF) ultrafiltration membranes via immersion–precipitation process. Surface characteristics of the membranes were confirmed by contact angle measurements, zeta potential, attenuated total reflectance Fourier transform infrared spectroscopy, X-ray photoelectron spectroscopy, scanning electron microscopy and atomic force microscopy. During filtration experiments, the modified membranes showed better permeation and antifouling performances compared to PVDF membranes with bovine serum albumin, sodium alginate and yeast. After hydraulic stirring cleaning with deionized water, water flux recovery and rejection ratio of the modified membranes were higher than those of pristine PVDF membrane, and the flux recovery ratio was maximized at 94.29%. It was suggested that PPG-co-PEG-co-PPG copolymer was anchored in the PVDF membrane through the two hydrophobic ends of PPG blocks, while the hydrophilic intermediate of the PEG block segregated onto the membrane or pore surface during the membrane preparation process. The synthesized method of amphiphilic PPG-co-PEG-co-PPG copolymer paved a novel way to solve the problems of less compatibility between the copolymer and membrane matrix and instability with water molecules in the ultrafiltration process.

Key words | amphiphilic copolymer, antifouling performance, poly(vinylidene fluoride) membrane, surface hydrophilicity

Bo Zhang
Po Gao (corresponding author)
School of Chemistry and Material Sciences,
Heilongjiang University,
Harbin, 150080,
China
E-mail: *1998022@hlju.edu.cn*

Panpan Wang
Haicheng Jiang
Jun Ma
State Key Laboratory of Urban Water Resource and Environment, School of Environments,
Harbin Institute of Technology,
Harbin 150090,
China

Jianxin Yu
Engineer Center of Analysis and Measurement,
Harbin Institute of Technology,
150001,
China

INTRODUCTION

Membrane separation technology has been widely used in the chemical industry, electronics, medicine, and environmental engineering (Ekambaram & Doraisamy 2016). The selection of membrane materials is an important aspect of membrane separation technology, which gained increasing attention in water treatment (Lu *et al.* 2017). Poly(vinylidene fluoride) (PVDF) membranes are popular in many applications owing to good membrane-forming and excellent physicochemical properties (Kang & Cao 2014). However, PVDF membranes have some limitations, especially owing to PVDF's intrinsic hydrophobicity. Organic pollutants are easily adsorbed onto the membrane surface or membrane pores in the filtration process (Boributh *et al.* 2009), resulting in membrane pore blockage, flux depression, and shortening of membrane life (Miao *et al.* 2017). It was widely accepted that surface hydrophilic modification was an efficient method to resist membrane fouling.

There are mainly two categories of modification methods for improving surface hydrophilicity and antifouling properties of PVDF membranes. The first category is to modify the membrane surface by surface grafting (Almasian *et al.* 2017), hydrophilic coating (Guo *et al.* 2018), plasma treatment (Tichonovas *et al.* 2013) and UV-induced grafting copolymerization (Anirudhan & Rejeena 2012). These

doi: 10.2166/wst.2019.203

modification methods change the pore distribution and hydrophilicity of the membrane surface, but require complex instrumentation and operating procedures, which also may cause flux decline due to pore blocking of contaminants on the membrane surface (Lü *et al.* 2016). Another category is carried out by adding surface-modifying molecules (SMMs) into the casting solution to improve hydrophilicity of the as-prepared membrane (Rana *et al.* 2005). This hydrophilic modification by SMMs is an *in situ* blending pathway and easily realized in industrial production lines, regardless of membrane materials and modules.

Two types of SMMs are commonly used for improving the hydrophilicity of membranes. The first type refers to water-soluble hydrophilic agents with small molecular weight, including polyethylene glycol (PEG) and polypropylene glycol (PPG) (Rajabzadeh *et al.* 2012). Arthanareeswaran and co-workers studied the effect of PEG 600 on ultrafiltration performance of polysulfone/sulfonated poly(ether ether ketone) membranes (Arthanareeswaran *et al.* 2010). With the increase of PEG 600 content from 2.5 to 7.5 wt%, the largest micropore size on the membrane surfaces increased from 38.9 to 42.7 Å. PEG has excellent ability to improve hydrophilicity interactions and unique coordination with surrounding water molecules (Tarboush *et al.* 2008). However, hydrophilic PEG with small molecular weight can easily leach out of the membrane matrix in the filtration process due to their high affinity with water (Liu *et al.* 2016).

Amphiphilic copolymer is another type of SMM. Rana and colleagues had successfully synthesized an end-capping urethane prepolymer by a two-step polymerization method and modified poly(ether sulfone) membranes (Rana *et al.* 2006). Statistical analysis showed that both moisture content and permeability had changed significantly. Tarboush *et al.* (2008) used hydrophilic SMMs to produce thin-film-composite polyamide membranes for the desalination of salty water. Dang and colleagues investigated the effect of hydrophilic SMMs blended with various host polymers on the performance of ultrafiltration membranes (Dang *et al.* 2010). It can be concluded that the two ends of SMMs are composed of hydrophilic segments of PEG, which made no stable cross-linking between the block copolymer and the membrane matrix, thus leading to no change in the contact angle and flux of the modified membranes. Up to now, the employment of two-hydrophobic end anchoring of copolymers does not appear in the literature on the preparation of blended polymeric membranes. Therefore, developing a simple and effective synthetic method of amphiphilic copolymer adapted to be compatible with the membrane matrix is the most essential assignment at present. Also, the stability in operation includes stability in fabrication and stability during the chemical cleaning. The stability in fabrication was reflected in the affinity of the matrix for the host hydrophobic polymer and it ensured that the copolymers were stably anchored to the PVDF membrane matrix. Therefore, the stability during chemical membrane cleaning should be one of the important topics to be studied in future.

In this work, we prepared a new amphiphilic copolymer which was blended into PVDF membranes to accomplish the purposes of improving water flux and enhancing antifouling performance with bovine serum albumin (BSA), sodium alginate (SA) and yeast solution. Systematically, structures of the synthesized amphiphilic copolymer were characterized. The performances of modified PVDF membranes were evaluated with regard to surface chemical construction, morphology, contact angle, zeta potential and antifouling property.

EXPERIMENTAL

Materials

The PVDF powder (average number-average molecular weight (M_n) = 380,000 g mol^{-1}) was provided by Shanghai 3F New Materials Co. Ltd. Analytical grade 4,4′-diphenylmethane diisocyanate (MDI), supplied by Aladdin Chemical Reagent Co., Ltd, N,N-dimethylacetamide (DMAc), PEG (M_n = 1,000 g mol^{-1}) and PPG (M_n = 2,000 g mol^{-1}) were purchased from Sigma Aldrich (Milwaukee, WI, USA). BSA (M_w = 67,000 g mol^{-1}) and SA were obtained from Sigma Chemical Co., Ltd. The yeast was obtained from China General Microbiological Culture. Deionized water was purified by distilled water with a Millipore Milli-Q filtration system.

Synthesis and characterization of copolymer

The PPG-co-PEG-co-PPG copolymer was synthesized by using the one-pot polymerization method in earlier reports (Rana *et al.* 2006). In the reaction, degassed PEG (2.0 g, 0.002 mol) with molecular weight of 1,000 was dissolved in dry DMAC solution in a round-bottom flask and stirred. After bubbling with nitrogen for 20 minutes, a mixture of MDI (0.75 g, 0.003 mol) and DMAC was added dropwise. The monomer was purged with N_2 gas for at least 30 minutes before adding DMAC to prevent the occurrence of side reactions. The higher molar ratio of MDI/PEG could ensure the end-capping by MDI. The structural verification of the

copolymer is shown in the 'Results and discussion' later. The flask was then placed in an oil bath heated to 80 °C and left for 7.5 h under nitrogen atmosphere. Then 0.002 mol PPG-2000 was dissolved in 20 mL degassed DMAc solvent with mechanical stirring at 80 °C for 8 h to obtain the resultant solution. After the reaction, the product was washed repeatedly for five times with deionized water to get the yellow precipitate; the precipitate was filtered and dried, then freeze-dried for 24 h. Fourier transform infrared (FTIR) spectra were recorded on a Perkin-Elmer spectrophotometer between 4,000 cm^{-1} and 500 cm^{-1}. To prepare FTIR samples, we used an agate mortar and pestle to grind the copolymer and mixed it with potassium bromide (KBr) (in a ratio of 1:100) to produce the powder, which was then pressed into a pellet. Proton nuclear magnetic resonance (^{1}H-NMR) spectra were recorded on a Bruker DRX 400 MHz spectrometer using dimethyl sulfoxide-d_6 as solvent.

Membrane preparation and characterization

The ultrafiltration membranes were obtained from casting solutions, containing PVDF graft copolymers in DMAC solution, by using the method of phase inversion (Wang *et al.* 2013). The compositions of the casting solution of the membrane are given in Supporting Information Table S2 (available with the online version of this paper). The PVDF powder, the solvent DMAC and additive were placed in a three-necked round-bottom flask and stirred for 4 hours in a constant temperature water bath at 70 °C. The casting was then allowed to stand at room temperature for 24 h to release air bubbles. The casting solution was evenly poured onto a glass plate, and the membrane was prepared using a casting knife with a thickness of 250 μm. The glass plate and membranes were immersed in deionized water at room temperature for more than 24 h to make the membranes separate from the solvent; then the membranes removed from the deionized water and dried at room temperature.

The attenuated total reflectance Fourier transform infrared spectroscopy (ATR-FTIR, Perkin-Elmer) was used for characterization of the chemical composition of the membranes. The sample membrane was dried before the test. It was important to obtain good contact between sample and the equipment. Contact angle of the membrane surface was measured by an OCA20 optical contact angle instrument (QSPJ 360). The surface zeta potential of the membrane was measured by a 1.0 mM KCL solution by a SurPASS electrokinetic analyzer (Anton-Paa) at a pH in the range of 2–9. Cross-sectional and surface morphologies were observed by scanning electron microscopy (S-4800) and surface topography was characterized by atomic force microscopy (AFM, Agilent 5100). The chemical elements on the membrane surface were analyzed by X-ray photoelectron spectroscopy (XPS, PHI 5700).

The overall porosity (ε) of the membrane was calculated from Equation (1):

$$\varepsilon(\%) = \frac{W_1 - W_2}{A \times l \times \rho} \times 100 \quad (1)$$

where A is the membrane area (m^2), l represents the thickness of the membrane (m), ρ is the density of water, W_1 is the wet weight of membrane, and W_2 is the dried weight of membrane.

Ultrafiltration experiments and antifouling properties evaluation

The pure water flux (J_w) was calculated according to Equation (2):

$$J_w = \frac{V}{A \times t} \quad (2)$$

where V means the volume of pure water through the membrane in a certain period time (L), A refers to the effective area of the membrane (m^2), t is the permeation time (h).

The real feed water quality composition is very complex, including organic pollutants, biological pollutants and particulate matter (Yamamura *et al.* 2014), and the main advantage of prepared membranes in this study is to resist and block the attack of organic contaminating molecules. BSA, SA and yeast solution are used as the model foulant to evaluate the permeation and antifouling property of prepared membranes (Zhao *et al.* 2014). In the progress of filtration experiments, the membranes were pre-compressed with the pressure of 0.15 MPa. Subsequently, pure water filtration was carried put for 30 minutes at the pressure of 0.1 MPa, the volume recorded as J_0, and then the flux for model foulant (0.2 g/L of BSA, SA, yeast solution) was measured as J_b at the pressure of 0.1 MPa. After the model foulant filtration, the membranes were washed with deionized water for 30 minutes, and then the volume of pure water was measured again, recorded as J_w. To further evaluate the antifouling properties of the membranes, the flux recovery ratio (*FRR*), total decline fouling ratio (DR_t), reversible decline fouling ratio (DR_r), and irreversible

decline fouling ratio (DR_{ir}) were investigated by Equations (3)–(6), respectively.

$$FRR(\%) = \frac{J_w}{J_0} \times 100 \quad (3)$$

$$DR_t\,(\%) = \frac{J_0 - J_b}{J_0} \times 100 \quad (4)$$

$$DR_r\,(\%) = \frac{J_w - J_b}{J_0} \times 100 \quad (5)$$

$$DR_{ir}\,(\%) = \frac{J_0 - J_w}{J_0} \times 100 \quad (6)$$

The rejection of model foulant was calculated according to the following equation via measuring the filtered solution with a UV-vis spectrophotometer; the rejection rate (R) was investigated by Equation (7):

$$R\,(\%) = \frac{C_f - C_p}{C_f} \times 100 \quad (7)$$

where C_p and C_f represent the concentrations of permeation solution and model foulant in the feed, respectively.

RESULTS AND DISCUSSION

Chemical analysis of copolymer PPG-co-PEG-co-PPG and membranes

Figure 1(b) shows the characteristic peaks of PEG, PPG and the synthetic copolymer PPG-co-PEG-co-PPG. As shown in Figure 1(b), the stretching vibration of the N–C=O appeared at 1,720 cm^{-1}, while those peaks at 1,279 cm^{-1} could designate the stretching vibration of C–N. For the PPG-co-PEG-co-PPG copolymers, the peaks corresponding to asymmetrical stretching vibrations of C–O bonds occurred at 1,130 cm^{-1}, in the spectra. Furthermore, the peak at 3,275 cm^{-1} was caused by the polyurethane stretching vibration of N–H and C=O in the copolymer, which demonstrated the successful polymerization of the MDI and PEG. The bands at 2,950 cm^{-1} were attributed to stretching vibration of C–H. Therefore, the presence of these signals could also indicate that PPG was responsive to macromolecules of the prepolymer. It was demonstrated that amphiphilic block copolymer PPG-co-PEG-co-PPG was successfully synthesized through the two-step polymerization

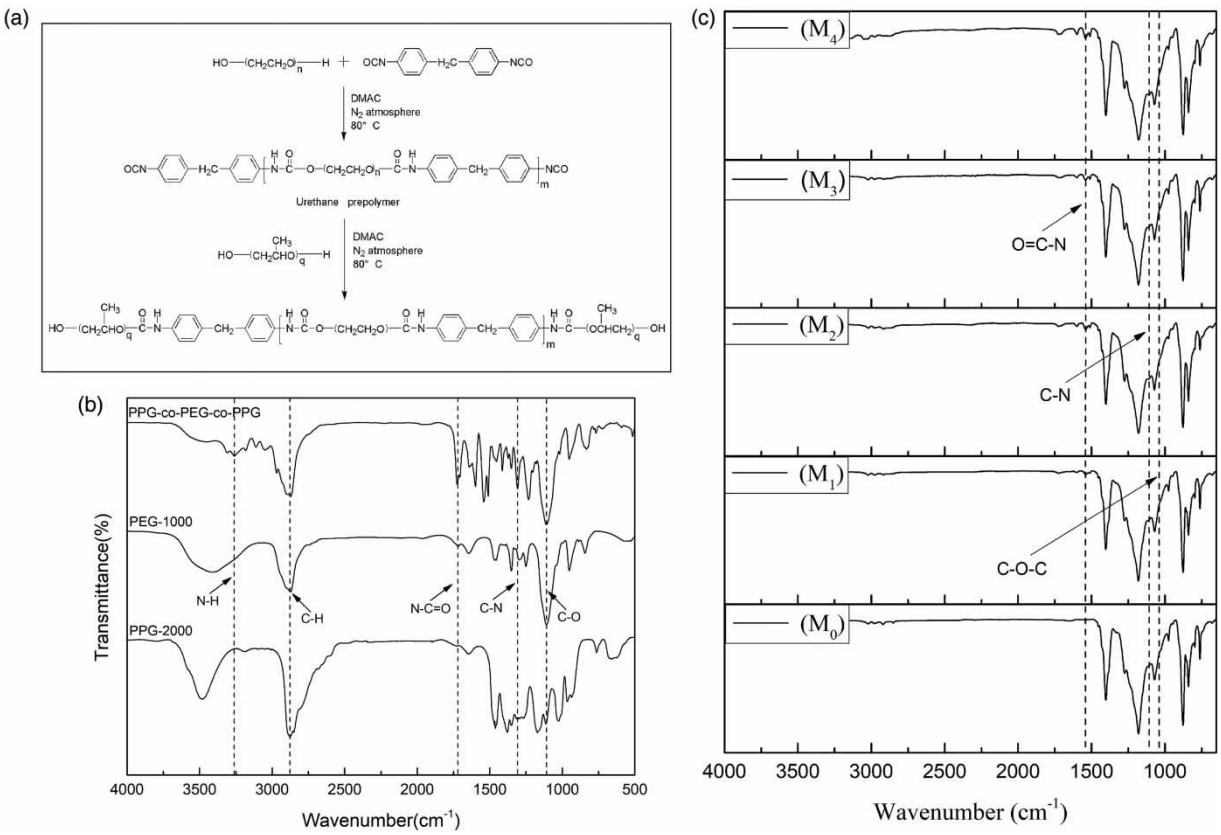

Figure 1 | (a) Schematic diagrams for the synthesis of PPG-co-PEG-co-PPG. (b) FTIR spectra of PPG-co-PEG-co-PPG copolymer, PEG-1000, and PPG-2000. (c) ATR-FTIR spectra of the membrane with pristine PVDF membrane (M_0) and modified membranes of PVDF/ PPG-co-PEG-co-PPG (M_1, M_2, M_3, and M_4).

process in Figure 1(a). The results of the NMR analysis also illustrated that the target copolymer was successfully produced. The characteristic peak of NH–CO group was at 8.09 ppm due to the terminal with –OH reacting successfully with the NCO in the prepolymer. Figure 1(c) shows the respective ATR-FTIR spectra for the top surface of the pristine PVDF membrane (M_0), and modified membranes with the PPG-co-PEG-co-PPG copolymer (M_1, M_2, M_3, M_4). Compared with pristine PVDF membrane, there were three new peaks in the spectra of modified membranes. The appearance of a stronger absorption at 1,580 cm^{-1} could be attributed to the O=C–N stretching vibration of the polyurethane in modified membranes (Sinha & Purkait 2015). As the concentration of the block copolymer gradually increased, the signal group of the O=C–N gradually became more pronounced. The other two stretching vibrations at 1,152 cm^{-1} and 1,080 cm^{-1} appeared in the spectra of the modified membranes, and these peaks represented the characteristic bands of C-N stretching mode and C-O-C bending vibrations, respectively (Carretier *et al.* 2016). The C–N stretching vibration was caused by the reaction of the NCO group with the hydroxyl group in the PEG or PPG. The results were consistent with the results of the subsequent XPS analysis. XPS analysis showed that the content of N and O elements increased with the addition of PPG-co-PEG-co-PPG copolymer. These characteristic bands confirmed the copolymer PPG-co-PEG-co-PPG had been successfully incorporated into the membrane surface.

Surface and morphological characterization of membranes

As can be seen from Figure 2, the integration of the additives changed the membrane formation process and affected the membrane surface and cross-sectional structure. The values of porosity of the pristine PVDF and PVDF/PPG-co-PEG-co-PPG membranes are presented in Table S1 (available with the online version of this paper). The cross-section of the pristine membrane exhibited a typical asymmetric structure with a skin layer, finger-like structure, and bottom supporting layer. After interfusing the copolymer, the macropore structure of the modified membranes extended to the entire cross-section. The prepared block copolymer PPG-co-PEG-co-PPG had a structure possessing a strong hydrophilic middle block and hydrophobic anchors at both end blocks, which was conducive to the increase in the number of pores and the pore size of the membrane surface, and the mean pore size of the membranes is shown in Table S3 (available online). It is well known that membrane properties can be controlled by many factors, including casting conditions and membrane morphology. The compatibility between casting solution and the coagulation bath was increased by interpolating hydrophilic polymer into the casting solution and speeding up the exchange rate between solvent and non-solvent, which was favorable for forming the large pores of the cross-section. The increase of pore size was beneficial to the transport of substances. However, the increase in the pore size was slow, and was not enough to cause membrane pore blockage on the membrane surface.

To further characterize the top surface topography of the modified and unmodified membranes, Figure 3 shows three-dimensional images of the AFM, and the surface roughness parameters of membranes are presented in Table S3. The AFM images included bright peak areas and darker valley areas. As the addition of block copolymers into casting solution increased, the modified membranes exhibited rougher surface topography, deeper grooves and more undulate peaks, while the root mean square ridge elevations of M_1, M_2, M_3 and M_4 increased to 1.34, 11.9, 17.3 nm and 22.1 nm respectively. Large roughness increased the total surface area of the dirt attached to the membrane, and the ridge–valley structure was generated due to the accumulation of surface fouling (Lalia *et al.* 2013). Particulate pollutants accumulated preferentially in the 'valley' of the rough membrane, resulting in 'valley blockage', which caused a serious drop in membrane flux. Smooth structured membranes were less prone to fouling than the relatively rough membranes (Elimelech *et al.* 1997). In addition, membrane fouling was also related to the zeta potential and contact angle of the membrane surface.

Contact angle and zeta potential analyses

The surface contact angle is an important parameter in surface hydrophilicity or hydrophobicity. Figure 4(a) shows the contact angles between the modified membranes and the pristine membrane. Compared with the pristine PVDF membrane, the contact angle of modified membranes had a significant decrease; the initial contact angle (M_0) of pristine PVDF membrane was about 87° while the initial contact angles of M_1, M_2, M_3 and M_4 decreased to 80°, 76°, 73° and 68° respectively. The study also examined the dynamic contact angles of the pristine PVDF membrane and modified membranes, the results of which are shown in Figure 4(b). Water contact angle of pristine membrane surface did not change obviously with time. In addition, the contact angles of the modified membranes decayed more significantly than that of the pristine PVDF membrane

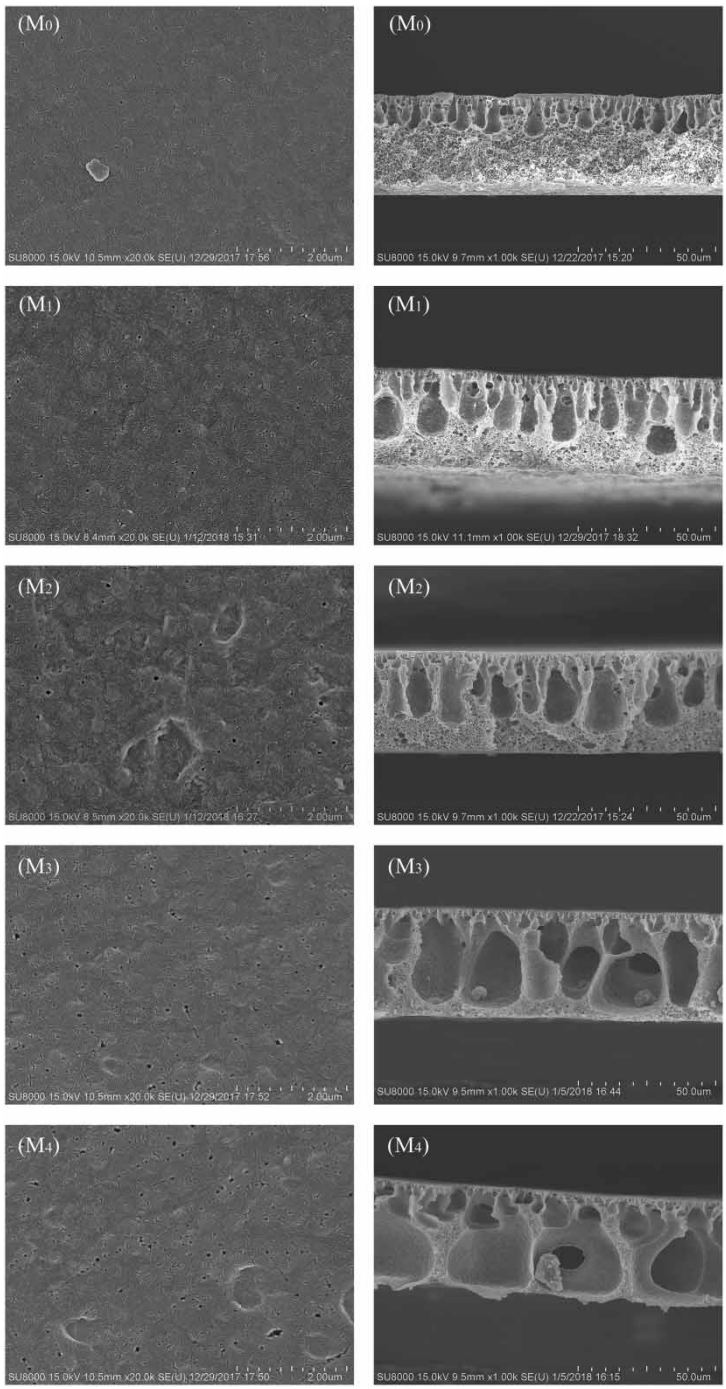

Figure 2 | Micrographs of the pristine PVDF (M_0) and modified membranes (M_1, M_2, M_3, and M_4). Left column: surface morphologies of membranes. Right column: cross-sections of membranes.

during the dripping time. The water contact angle depends not only on the surface wettability but also on the surface roughness (Xu *et al.* 2015). Theoretical and experimental studies have concluded that, for most surfaces, roughness below a certain threshold (usually <100 nm) usually does not affect the hysteresis of the contact angle (Extrand 2004). It confirmed that the combination of the hydrophilic copolymer into the membrane matrix enhanced the hydrophilicity of the membrane surface. The surface zeta potential of PVDF and M_2 and M_4 changes with pH as shown in Figure 4(c). The membrane potential showed positive charge at low pH and negative charge at high pH. The

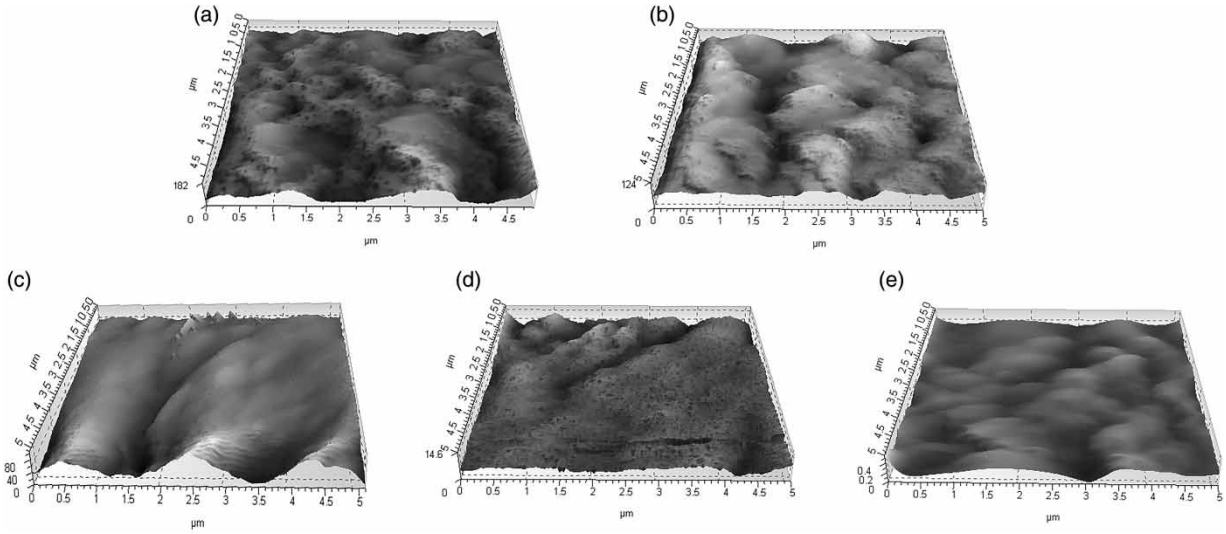

Figure 3 | AFM three-dimensional images of membrane surfaces of the pristine PVDF (M_0) (a) and modified membranes M_1, M_2, M_3, and M_4 ((b) to (e), respectively).

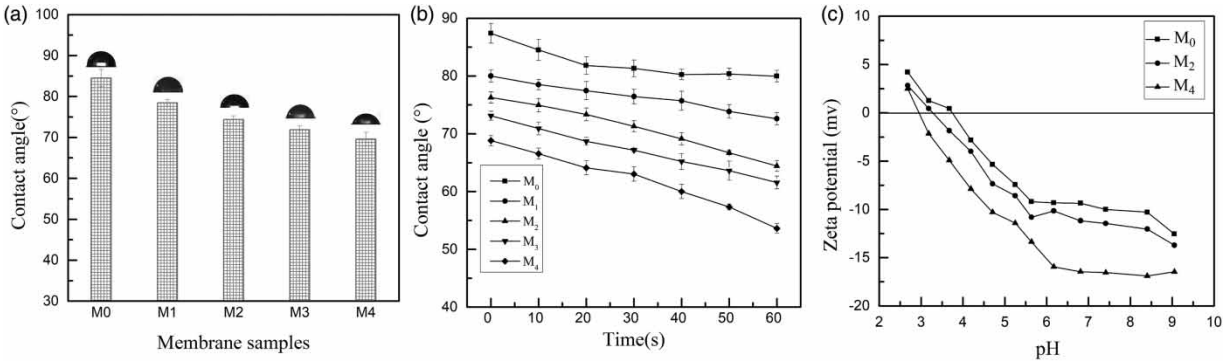

Figure 4 | (a) Water contact angles of the pristine PVDF (M_0) and modified membranes (M_1, M_2, M_3, and M_4), (b) variation in water contact angle during dripping time and (c) surface zeta potentials of the PVDF membrane and modified membranes (M_2 and M_4).

modified membranes exhibited even more negative zeta potential than the original membrane, which may be attributed to the ether group in the PEG molecule adsorbing the hydroxyl ion through hydrogen bonding. The modified membrane M_4 had a large number of negatively charged hydroxyl groups, so modified membrane M_4 showed the lowest electronegativity. The increase in the negative charge resulted in the pollution particles (such as proteins) with similar pore size and negative charge on the surface of the membrane being further increased. In addition, electrostatic repulsion between the membrane and the functional group also caused the reduction of membrane fouling.

XPS analyses

The element analyses of copolymer coverages on the membrane surface were confirmed by XPS, as shown in Figure 5. In Figure 5(a), the typical characteristic peaks of pristine PVDF membrane were located at around 685.3 eV for F1s and 286.4 eV for C 1s. Differing from that of the pristine PVDF membrane, two new peaks of N element and O element were observed in the wide scan spectra of modified membranes, corresponding to the signals with binding energies of 401.8 eV and 533.2 eV in the copolymer, respectively. The chemical composition of the membrane surface is listed in Table S1. Obviously, the content of nitrogen and oxygen elements was significantly increased, while the decrease of fluorine element was observed compared to the pristine membrane. In addition, the experimental values of N/F for modified membranes were much higher than the theoretical values. The hydrophilic groups were concentrated on the surface of the membrane, and hydrophobic groups were embedded in the membrane matrix. We obtained the C 1s core-level spectra of the pristine

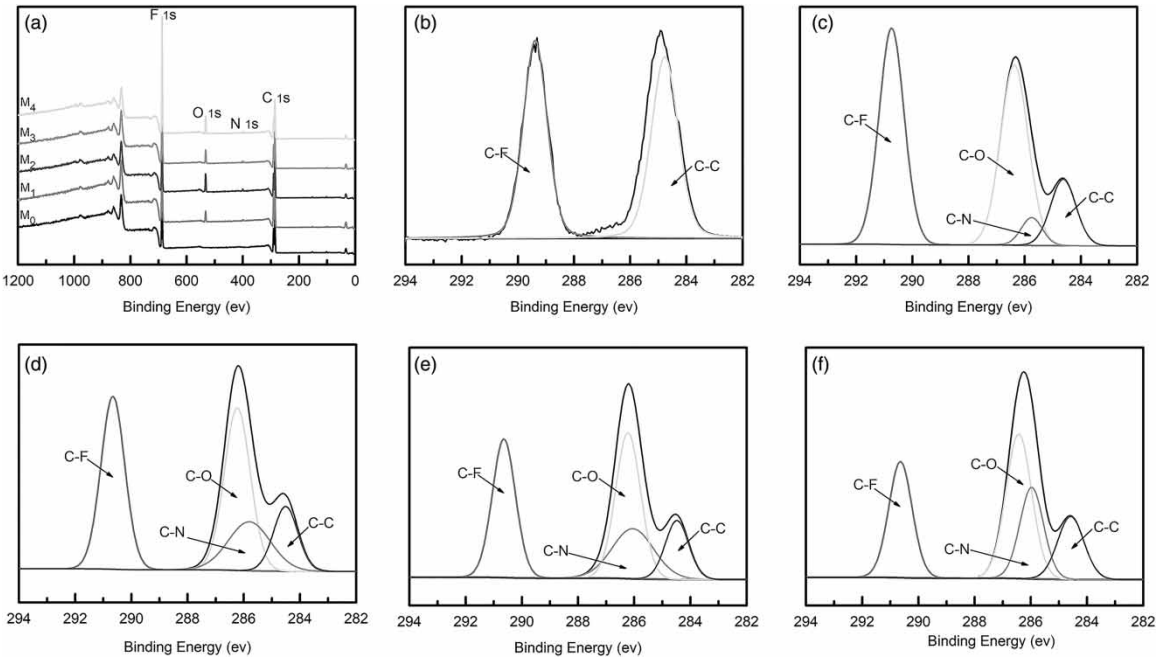

Figure 5 | (a) Wide-scan XPS spectra of the pristine PVDF (M_0) and modified membranes (M_1, M_2, M_3, and M_4). C 1s core-level spectra of (b) membrane M_0, (c) membrane M_1, (d) membrane M_2, (e) membrane M_3, and (f) membrane M_4.

membrane (M_0) and modified membranes (M_1, M_2, M_3, and M_4), in which two or three peaks differentiation were fitted by curve-fitted analysis. Simultaneously, the pristine PVDF membrane only showed carbon and fluorine signal components with binding energies at 284.6 eV and 290.1 eV, as presented in Figure 5(b). Meanwhile, there were typical oxygen peaks and nitrogen peaks in the modified membranes, and the binding energies at 286.5 eV and 285.8 eV respectively. The new peaks of the nitrogen element in the modified membranes demonstrated that PPG-co-PEG-co-PPG copolymer had been distributed into the modified PVDF membrane.

Antifouling property

Antifouling property of PVDF/PPG-co-PEG-co-PPG membranes was evaluated, according to the changes of water flux. *FRR* is an indicator of reversibility of membrane fouling. Figure 6 shows the change tendency in water flux and fouling-resistant behavior of membranes during the cycle filtration. From Figure 6(a), the water flux of PVDF/PPG-co-PEG-co-PPG ultrafiltration membranes showed a decreasing trend in varying degrees and maintained a stable level with the filtration process of BSA aqueous solution after 20 minutes. After a simple hydraulic stirring cleaning, the flux of water permeation increased significantly. The *FRR* values are calculated as 70.88%, 82.06%, 93.33%, 94.81% and 94.29% respectively for the M_0, M_1, M_2, M_3 and M_4 membranes. As seen from Figure 6(b) and 6(c), all modified membranes had higher water flux and flux recovery rate than the pristine PVDF membrane after filtration with SA and yeast solution. In Figure 6(c), after a moment of membrane flux measured, M_4 membrane was not stable due to pressure instability (pre-pressure 0.15 MPa conversion to 0.1 MPa), and the flux of M_4 membrane had a stable state after the pressure stabilized at 0.1 MPa. The rejection rate (R%) of membranes is shown in Table S4 (available online). The rejection rate of a pristine membrane was 68.5% while the BSA rejection of modified membranes of M_1, M_2, M_3 and M_4 increased to 76.8%, 80.6%, 85.2%, and 95.4%, respectively. The antifouling properties were remarkably improved and the SA and yeast rejection was maintained at a high level for modified M_4 membranes (>99%). The hydrophilic groups in PPG-co-PEG-co-PPG copolymer inhibited and reduced the adhesion caused by the non-specific interaction between the pollutants and membrane surface, making the membrane block the attack of pollutants. With the increased amounts of copolymer PPG-co-PEG-co-PPG, the water permeation flux increased and attained its maximum at PPG-co-PEG-co-PPG of 2.0 wt%. Antifouling membranes fabricated via different modified methods are briefly summarized in

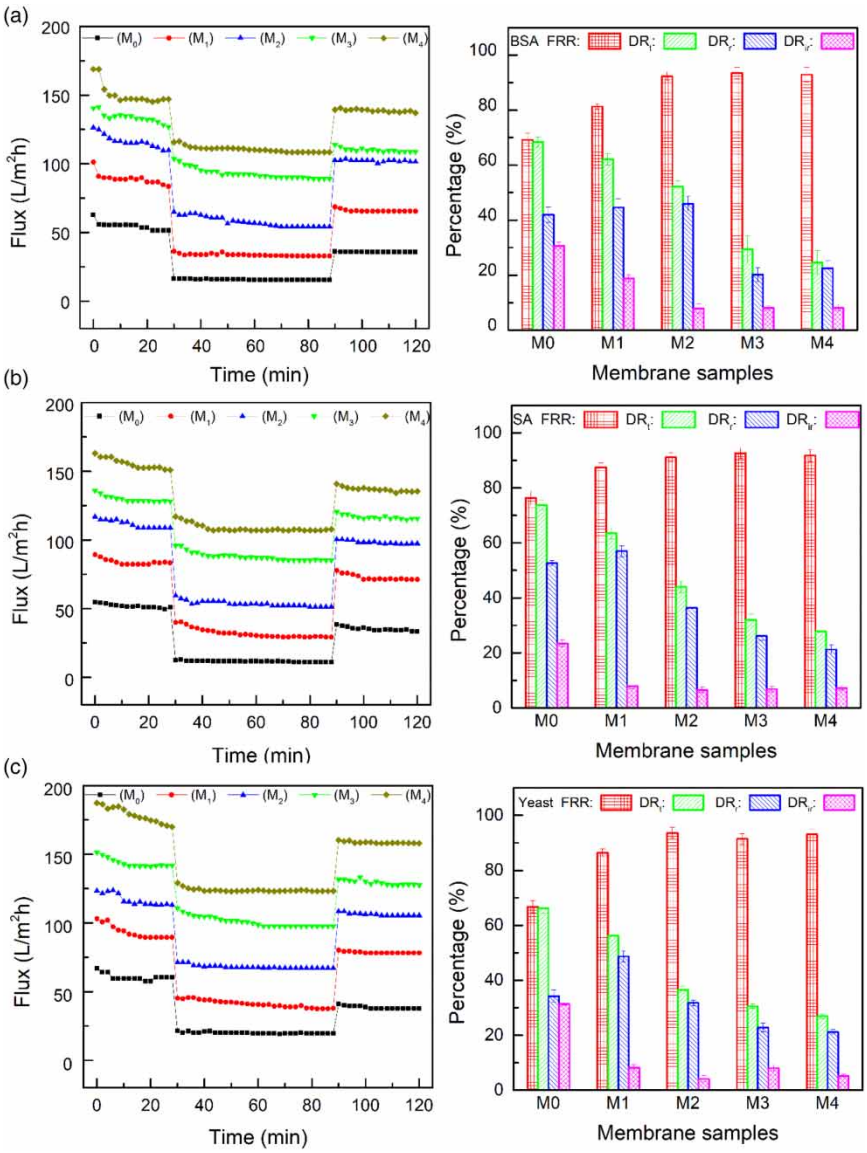

Figure 6 | Left column: time dependence on recycling flux for the M_0, M_1, M_2, M_3 and M_4 membranes during the filtration of (a) BSA solution, (b) SA solution, and (c) yeast solution. Right column: summary of total fouling ratio (R_t), irreversible ratio (R_{ir}), reversible fouling ratio (R_r), and flux recovery ratio (FRR) during the cycle filtration.

Table 1. It is observed from this table that PVDF/PPG-co-PEG-co-PPG membrane showed excellent antifouling performance during the filtration of 0.2 g/L of BSA, SA and yeast solution. PPG-co-PEG-co-PPG copolymer incorporated into the membrane casting solution promoted the increase in the number of membrane pores and pore size. In addition, the PEG hydrophilic segment on the surface of the modified membrane could form a hydration layer by hydrogen bonding, which acted as a protective layer between the pollutants and membrane surface (Hashim *et al.* 2009). The stability during the chemical cleaning depends on the anchoring effect and chemical resistance of the amphiphilic block polymer. The stability during chemical membrane cleaning should be an important subject in the future study.

CONCLUSION

A simple and effective method to improve the hydrophilicity and antifouling resistance of PVDF membrane surface was successfully developed. We carried out the synthesis of copolymer PPG-co-PEG-co-PPG with superior properties via one-pot polymerization reaction in this study. Blending of the amphiphilic copolymer and PVDF powders was

Table 1 | Antifouling performance comparison between this work and other modified membranes

Membrane	Pure water flux (L/m^2 h)	Organic feed	Rejection (%)	FRR (%)	Reference
Ag/SiO_2-modified PVDF	~410	0.2 g/L BSA	75	50.2	Pan *et al.* (2016)
GO-modified PVDF	166	0.1 g/L BSA	84	92	Zhang *et al.* (2013)
PU-modified PVDF	~169	1.0 g/L BSA	88	93	Lü *et al.* (2016)
CNC-modified PVDF	40	0.2 g/L BSA	82	~79	Lv *et al.* (2018)
HEA-grafted PVDF	486	0.1 g/L SA	–	92	Shen *et al.* (2018)
PVC-PEGMA blended PVC	461	2 g/L SA	94	80	Wu *et al.* (2018)
PHFBM-PMAA-PMTAC PVDF	120	0.1 g/L yeast	99	94	Wang *et al.* (2019)
PBI-modified PSF	355	0.05 M BSA	~69	~93	Eren *et al.* (2015)
PVDF/PPG-PEG-PPG (M_4)	171	0.2 g/L BSA	95	94	In this work
PVDF/PPG-PEG-PPG (M_4)	164	0.2 g/L SA	99	90.8	In this work
PVDF/PPG-PEG-PPG (M_4)	182	0.2 g/L yeast	99	93.2	In this work

GO, graphene oxide; PU, polyurethane; CNC, cellulose nanocrystal; HEA, hydroxyethyl acrylate; PVC, polyvinyl chloride; PEGMA, poly(ethylene glycol) methyl ether methacrylate; PHFBM-PMAA-PMTAC, poly(hexafluorobutyl methacrylate)-poly(methacrylic acid)-poly[(2-(methacryloyloxy) ethyl) trimethyl ammonium chloride]; PBI, poly[2,2′-(m-phenylene)-5,5′-dibenzimidazole]; PSF, polysulfone.

used to prepare hydrophilic PVDF/PPG-co-PEG-co-PPG membrane through the immersion–precipitation process. Filtration experiments showed that the resulting membranes were more effective in preventing and releasing model foulants such as BSA, SA and yeast solution. More importantly, the flux recovery rate and irreversible fouling rate both increased significantly with the incorporation of PPG-co-PEG-co-PPG. Compared with the pristine membrane, both total fouling ratio and irreversible fouling ratio decreased significantly. Among them, the flux recovery rate of M_4 membrane reached as high as 94.29%, and the rejection rate reached more than 99%. Therefore, the novel PVDF/PPG-co-PEG-co-PPG membranes may lay the foundation for antifouling membranes with wide applicability.

ACKNOWLEDGEMENTS

This work was financially supported by China Postdoctoral Science Foundation (Grant No. 2017M611377), National Natural Science Foundation of China (Grant No. 51508129), National Key R&D Program of China (Grant No. 2017YFA0207203), National Science and Technology Major Projects for Water Pollution Control and Treatment (Grant No. 2017ZX07201003).

REFERENCES

Almasian, A., Jalali, M. L., Fard, G. C. & Maleknia, L. 2017 Surfactant grafted PDA-PAN nanofiber: optimization of synthesis, characterization and oil absorption property. *Chemical Engineering Journal* **326**, 1232–1241.

Anirudhan, T. S. & Rejeena, S. R. 2012 Poly(acrylic acid)-modified poly(glycidylmethacrylate)-grafted nanocellulose as matrices for the adsorption of lysozyme from aqueous solutions. *Chemical Engineering Journal* **187**, 150–159.

Arthanareeswaran, G., Mohan, D. & Raajenthiren, M. 2010 Preparation, characterization and performance studies of ultrafiltration membranes with polymeric additive. *Journal of Membrane Science* **350**, 130–138.

Boributh, S., Chanachai, A. & Jiraratananon, R. 2009 Modification of PVDF membrane by chitosan solution for reducing protein fouling. *Journal of Membrane Science* **342**, 97–104.

Carretier, S., Chen, L.-A., Venault, A., Yang, Z.-R., Aimar, P. & Chang, Y. 2016 Design of PVDF/PEGMA-b-PS-b-PEGMA membranes by VIPS for improved biofouling mitigation. *Journal of Membrane Science* **510**, 355–369.

Dang, H. T., Amelot, C., Rana, D., Narbaitz, R. M. & Matsuura, T. 2010 Performance of a newly developed hydrophilic additive blended with different ultrafiltration base polymers. *Journal of Applied Polymer Science* **116**, 2205–2215.

Ekambaram, K. & Doraisamy, M. 2016 Study on the fabrication, characterization and performance of PVDF/calcium stearate composite nanofiltration membranes. *Desalination* **385**, 24–38.

Elimelech, M., Xiaohua, Z., Childress, A. E. & Seungkwan, H. 1997 Role of membrane surface morphology in colloidal fouling of cellulose acetate and composite aromatic polyamide reverse osmosis membranes. *Journal of Membrane Science* **127**, 101–109.

Eren, E., Sarihan, A., Eren, B., Gumus, H. & Kocak, F. O. 2015 Preparation, characterization and performance enhancement of polysulfone ultrafiltration membrane using PBI as hydrophilic modifier. *Journal of Membrane Science* **475**, 1–8.

Extrand, C. W. 2004 Contact angles and their hysteresis as a measure of liquid–solid adhesion. *Langmuir* **20**, 4017–4021.

Guo, H., Xu, T., Zhang, J., Zhao, W., Zhang, J., Lin, C. & Zhang, L. 2018 A multifunctional anti-fog, antibacterial, and self-cleaning surface coating based on poly(NVP-co-MA). *Chemical Engineering Journal* **351**, 409–417.

Hashim, N. A., Liu, F. & Li, K. 2009 A simplified method for preparation of hydrophilic PVDF membranes from an amphiphilic graft copolymer. *Journal of Membrane Science* **345**, 134–141.

Kang, G.-d. & Cao, Y.-m. 2014 Application and modification of poly(vinylidene fluoride) (PVDF) membranes – a review. *Journal of Membrane Science* **463**, 145–165.

Lalia, B. S., Kochkodan, V., Hashaikeh, R. & Hilal, N. 2013 A review on membrane fabrication: structure, properties and performance relationship. *Desalination* **326**, 77–95.

Liu, J., Ma, Y., Gao, B., Meng, H., Yu, L. & Wang, L. 2016 Ammonium persulphate as novel additive for filtration performance improvement of PVDF microporous membrane. *Separation and Purification Technology* **165**, 78–85.

Lü, X., Wang, X., Guo, L., Zhang, Q., Guo, X. & Li, L. 2016 Preparation of PU modified PVDF antifouling membrane and its hydrophilic performance. *Journal of Membrane Science* **520**, 933–940.

Lu, T., Xu, X., Liu, X. & Sun, T. 2017 Super hydrophilic PVDF based composite membrane for efficient separation of tetracycline. *Chemical Engineering Journal* **308**, 151–159.

Lv, J., Zhang, G., Zhang, H., Zhao, C. & Yang, F. 2018 Improvement of antifouling performances for modified PVDF ultrafiltration membrane with hydrophilic cellulose nanocrystal. *Applied Surface Science* **440**, 1091–1100.

Miao, W., Li, Z.-K., Yan, X., Guo, Y.-J. & Lang, W.-Z. 2017 Improved ultrafiltration performance and chlorine resistance of PVDF hollow fiber membranes via doping with sulfonated graphene oxide. *Chemical Engineering Journal* **317**, 901–912.

Pan, Y., Yu, Z., Shi, H., Chen, Q., Zeng, G., Di, H., Ren, X. & He, Y. 2016 A novel antifouling and antibacterial surface-functionalized PVDF ultrafiltration membrane via binding Ag/SiO_2 nanocomposites. *Journal of Chemical Technology & Biotechnology* **92**, 562–572.

Rajabzadeh, S., Liang, C., Ohmukai, Y., Maruyama, T. & Matsuyama, H. 2012 Effect of additives on the morphology and properties of poly(vinylidene fluoride) blend hollow fiber membrane prepared by the thermally induced phase separation method. *Journal of Membrane Science* **423–424**, 189–194.

Rana, D., Matsuura, T., Narbaitz, R. M. & Feng, C. 2005 Development and characterization of novel hydrophilic surface modifying macromolecule for polymeric membranes. *Journal of Membrane Science* **249**, 103–112.

Rana, D., Matsuura, T. & Narbaitz, R. M. 2006 Novel hydrophilic surface modifying macromolecules for polymeric membranes: polyurethane ends capped by hydroxy group. *Journal of Membrane Science* **282**, 205–216.

Shen, L., Wang, H., Zhang, Y., Li, R., Fabien, B., Yu, G., Lin, H. & Liao, B.-Q. 2018 New strategy of grafting hydroxyethyl acrylate (HEA) via γ ray radiation to modify polyvinylidene fluoride (PVDF) membrane: thermodynamic mechanisms of the improved antifouling performance. *Separation and Purification Technology* **207**, 83–91.

Sinha, M. K. & Purkait, M. K. 2015 Preparation of fouling resistant PSF flat sheet UF membrane using amphiphilic polyurethane macromolecules. *Desalination* **355**, 155–168.

Tarboush, B. J. A., Rana, D., Matsuura, T., Arafat, H. A. & Narbaitz, R. M. 2008 Preparation of thin-film-composite polyamide membranes for desalination using novel hydrophilic surface modifying macromolecules. *Journal of Membrane Science* **325**, 166–175.

Tichonovas, M., Krugly, E., Racys, V., Hippler, R., Kauneliene, V., Stasiulaitiene, I. & Martuzevicius, D. 2013 Degradation of various textile dyes as wastewater pollutants under dielectric barrier discharge plasma treatment. *Chemical Engineering Journal* **229**, 9–19.

Wang, P., Ma, J., Shi, F., Ma, Y., Wang, Z. & Zhao, X. 2013 Behaviors and effects of differing dimensional nanomaterials in water filtration membranes through the classical phase inversion process: a review. *Industrial & Engineering Chemistry Research* **52**, 10355–10363.

Wang, F., He, M., Gao, K., Su, Y., Zhang, R., Liu, Y., Shen, J., Jiang, Z. & Kasher, R. 2019 Constructing membrane surface with synergistic passive antifouling and active antibacterial strategies through organic-inorganic composite modifier. *Journal of Membrane Science* **576**, 150–160.

Wu, H., Li, T., Liu, B., Chen, C., Wang, S. & Crittenden, J. C. 2018 Blended PVC/PVC-g-PEGMA ultrafiltration membranes with enhanced performance and antifouling properties. *Applied Surface Science* **455**, 987–996.

Xu, Z., Zhao, Y., Wang, H., Wang, X. & Lin, T. 2015 A superamphiphobic coating with an ammonia-triggered transition to superhydrophilic and superoleophobic for oil–water separation. *Angewandte Chemie International Edition* **54**, 4527–4530.

Yamamura, H., Okimoto, K., Kimura, K. & Watanabe, Y. 2014 Hydrophilic fraction of natural organic matter causing irreversible fouling of microfiltration and ultrafiltration membranes. *Water Research* **54**, 123–136.

Zhang, J., Xu, Z., Mai, W., Min, C., Zhou, B., Shan, M., Li, Y., Yang, C., Wang, Z. & Qian, X. 2013 Improved hydrophilicity, permeability, antifouling and mechanical performance of PVDF composite ultrafiltration membranes tailored by oxidized low-dimensional carbon nanomaterials. *Journal of Materials Chemistry A* **1**, 3101–3111.

Zhao, X., Su, Y., Li, Y., Zhang, R., Zhao, J. & Jiang, Z. 2014 Engineering amphiphilic membrane surfaces based on PEO and PDMS segments for improved antifouling performances. *Journal of Membrane Science* **450**, 111–123.

First received 9 August 2018; accepted in revised form 9 June 2019. Available online 17 June 2019